A Novel In-Service Measurement Technique Using the Same Wavelength Band as SCM Signals

Fumihiko Yamamoto and Tsuneo Horiguchi, *Senior Member, IEEE, Member, OSA*

***Abstract*—This paper proposes a new technique for measuring in-service optical fibers, that uses an optical time domain reflectometer (OTDR). The feature of the proposed technique is that the OTDR light is in the same wavelength band as the video signal, which is distributed by using the subcarrier multiplexing (SCM) technique. In a 40-channel SCM system operating at a signal wavelength of 1.558 μm, we show that the required video quality can be maintained, by using the proposed OTDR operating in the 1.55 μm band, even though the measured fiber is in service and the OTDR light enters an optical receiver. Moreover, we clarify the conditions for undertaking measurements, without the need for optical filters designed to prevent OTDR light from degrading the SCM signal quality.**

***Index Terms*—In-service testing, optical time domain reflectometer (OTDR), SCM.**

I. Introduction

RECENTLY, subcarrier multiplexing (SCM) optical transmission has been researched and developed as an important multiplexing technique for high-capacity lightwave systems [1]–[3]. Erbium-doped fiber amplifiers (EDFA) are used to increase the transmission distance or distribution number, using a passive double star network (PDSN) in an SCM system, therefore the wavelength of the transmitted video signal is in the 1.55-μm region.

An optical time domain reflectometer (OTDR), installed in a central office, is used when remotely measuring the optical fiber lines by which video services are provided in the PDSN [4], [5]. The measurement wavelength is in the 1.6-μm band, which is different from that of the video signal. Moreover, a short wavelength pass filter (SWPF) is positioned at the input port of each optical network unit (ONU). Therefore, the video service quality does not degrade, even though the video signal and an optical pulse from the OTDR propagate simultaneously in an optical fiber. However, fiber line, splice and connector return losses at 1.55 μm are estimated from data measured at 1.6 μm with that technique, and there may be errors in the estimation.

This paper proposes a new in-service measurement technique, that uses the same wavelength band as the carrier signal of an SCM system, without interrupting amplitude modulated (AM) vestigial sideband signal services. By using the new technique, it is possible to evaluate the transmission line characteristics accurately, since the loss data are obtained directly without the need for estimation. The SWPFs therefore can be removed from optical lines, thus reducing the system cost. Section II discusses the basic principles of suppressing additional noise caused within the SCM signal band when OTDR light enters an ONU. In Section III, we measure the quantitative behavior of the carrier-to-noise ratio (CNR) to show the feasibility of the proposed OTDR in a 40-channel lightwave AM-SCM system, and discuss the conditions for eliminating SWPFs from optical networks. We also show the characteristics of the new OTDR. Finally, Section IV is devoted to the spatial resolution of the OTDR, as regards the new in-service measurement system.

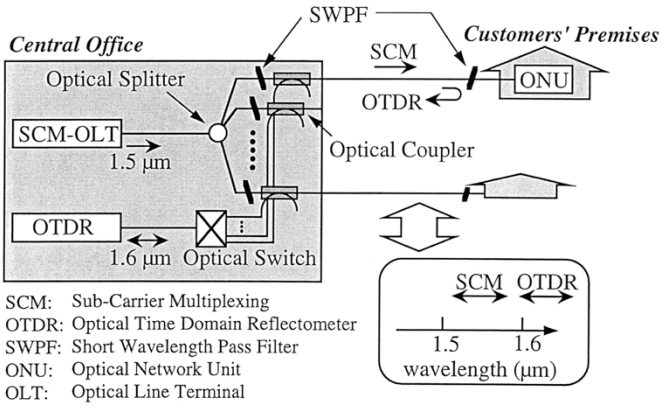

Fig. 1. Configuration of a conventional in-service measurement system in an SCM system.

II. Suppression of Extra Noise Due to OTDR Light

Fig. 1 shows a conventional in-service measurement system, in which SCM signals propagate in optical fiber lines. Since the wavelength region of the OTDR pulses is different from that of the SCM signals, the pulses can be cut by using an SWPF in front of an ONU. Therefore, OTDR measurements can be undertaken, even when the test fiber is in service. If the OTDR light enters the ONU, there is extra noise within the signal band, P_{OTDR}, as follows:

$$P_{\mathrm{OTDR}} = P_{\mathrm{pulse}} + P_{\mathrm{RIN}} + P_{\mathrm{shot}}. \tag{1}$$

The first term is responsible for the frequency components of the OTDR pulse waveform. The second term results from the intensity fluctuations in the OTDR light, for example mode partition noise. The third term represents shot noise. To measure in-service fibers using the same wavelength band as the video signal, we must keep these extra noises at a low level because the SWPF cannot prevent the OTDR light from entering the ONU.

Manuscript received January 26, 2000; revised June 22, 2000.

The authors are with the NTT Access Network Service Systems Laboratories, Ibaraki 305-0805, JAPAN.

Publisher Item Identifier S 0733-8724(00)09097-6.

0733–8724/00$10.00 © 2000 IEEE

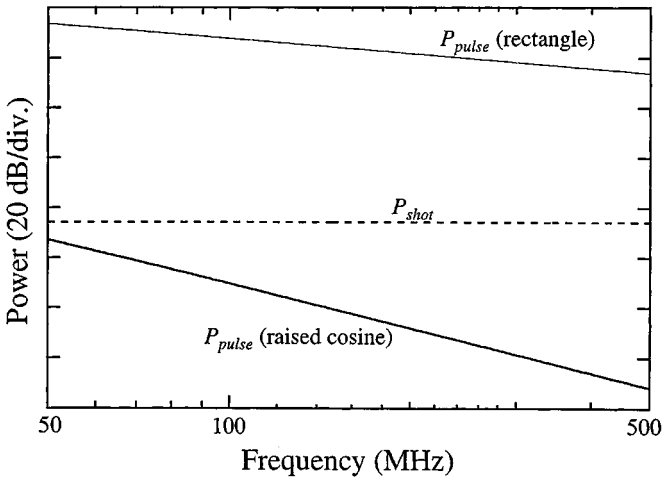

Fig. 2. Variation of pulse-induced noise with frequency at a pulse width of 1 μs. The solid and light solid lines show the theoretical variation for raised cosine and rectangular waveforms, respectively. The dashed line shows the shot noise when it is assumed to be independent of frequency.

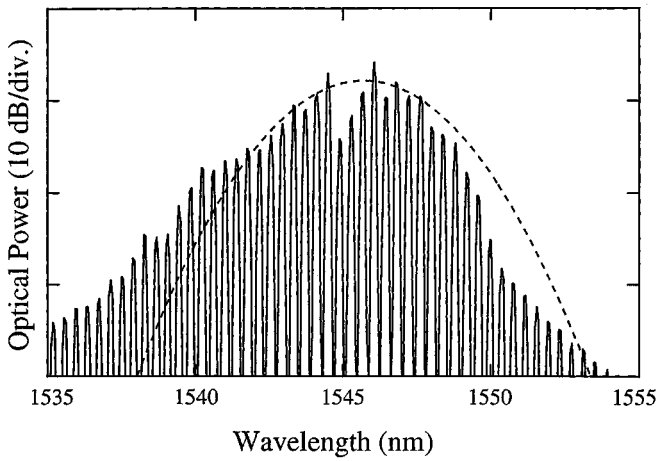

Fig. 3. Average optical spectrum of an FP-LD with a center wavelength of 1546 nm and a mode spacing of 0.4 nm. It is directly modulated into pulse trains with a pulse width of 1-μs and a repetition cycle of 430-μs, and is measured using an optical spectrum analyzer with a resolution bandwidth of 0.1 nm. When the spectrum is assumed to obey a Gaussian distribution as shown with a dashed line, the FWHM is 4.7 nm.

A. OTDR Pulse-Induced Noise

When the sidelobes of a pulse frequency spectrum are superimposed on the subcarrier frequency band, they degrade the video quality. Therefore, the quantitative behavior depends on the pulse waveform. When the OTDR light is received at an ONU, the pulse-induced noise power in one subcarrier frequency band is given by [5]

$$P_{\rm pulse} = \frac{1}{2}(\max\cdot[|n_{\rm pulse}(t)|])^2 \cdot (\rho P_{\rm peak})^2 R_D G, \quad (2)$$

where $n_{\rm pulse}(t)$ is the temporal response function of a pulse train passing through one subcarrier band, ρ is the responsivity of the photodiode (PD) of the ONU, $P_{\rm peak}$ is the optical peak power of the OTDR light at the ONU, R_D is the input resistance of the ONU, and G is the electrical power gain in the ONU. $n_{\rm pulse}(t)$ is related to the Fourier transform of the pulse waveform from an OTDR $F_{\rm pulse}(f)$ and the reciprocal of the OTDR pulse repetition cycle f_R as

$$n_{\rm pulse}(t) = 2f_R \cdot \sum_{n=n_1}^{n_2} F_{\rm pulse}(nf_R) \cdot \cos(2\pi n f_R t), \quad (3)$$

with

$$n_1 = f_c/f_R + \varepsilon_1, \quad n_2 = (f_c + B_W)/f_R + \varepsilon_2, \quad |\varepsilon_{1,2}| < 1/2. \quad (4)$$

where n_1 and n_2 are integers, and f_c and B_W are the subcarrier frequency and its signal bandwidth, respectively.

Subcarrier frequencies are usually in the high frequency region, namely above 90 MHz. Therefore, it is very effective to compress the pulse spectrum and arrange it below the minimum subcarrier frequency to reduce the pulse-induced noise. When the pulse waveform, $n_{\rm rc}(t)$, from an OTDR is a raised cosine as

$$n_{\rm rc}(t) = \begin{cases} \frac{1}{2}[1 + \cos(\pi/T_P \cdot t)] & (-T_P \le t \le T_P) \\ 0 & (\text{otherwise}) \end{cases} \quad (5)$$

and not a rectangle (conventional OTDR waveform), the pulse-induced noise can be reduced in the subcarrier frequency band. Here, T_P in (5) corresponds to the pulse width. Fig. 2 shows the pulse-induced noise power $P_{\rm pulse}$ as a function of the frequency at $P_{\rm peak} = 0$ dBm, $B_W = 4.2$ MHz, $\rho = 0.85$, and $f_R = 1/430$ MHz. The solid line is the theoretical prediction of (2) for the raised cosine waveform. At the minimum subcarrier frequency of 90 MHz, the pulse-induced noise power decreases by 96 dB, compared with that of the rectangular waveform shown with the light solid line. The most notable feature is that the pulse-induced noise power of the raised cosine waveform is suppressed below the shot noise power, $P_{\rm shot}$, of the pulse train over the subcarrier frequencies under the calculation conditions.

B. Intensity Fluctuation Noise

Since a Fabry–Perot laser diode (FP-LD) can easily provide high output powers, it is commonly used as an OTDR light source. The FP-LD has many longitudinal modes, as shown in Fig. 3, and the power distribution among the different longitudinal modes fluctuates randomly, even when the total emitted power is constant. Therefore, mode partition noise occurs with the dispersion of fibers when the light from the OTDR propagates into the fibers [6]. As a result, the intensity fluctuation noise depends not only on the intrinsic intensity noise of the light source, but also on the mode partition noise. The fluctuation noise in one subcarrier frequency band $P_{\rm RIN}$ is given by

$$P_{\rm RIN} = (\rho \cdot P_{\rm peak})^2 R_D G \sum_{k=1}^{2} d \cdot {\rm RIN}_k \cdot B_W \quad (6)$$

where d is the duty ratio of the OTDR pulse train, and $\rm RIN_1$ and $\rm RIN_2$ are the relative intensity noise (RIN) of an OTDR light source and mode partition noise, respectively.

Fig. 4 shows the observed variation in the mode partition noise with frequency in an experiment where 1.55-μm light with the spectrum, shown in Fig. 3, is transmitted over a 10-km long single-mode (SM) fiber with a zero-dispersion wavelength of 1.3 μm. Since the noise values are larger than those of the intrinsic noise, it is very important to reduce the mode partition

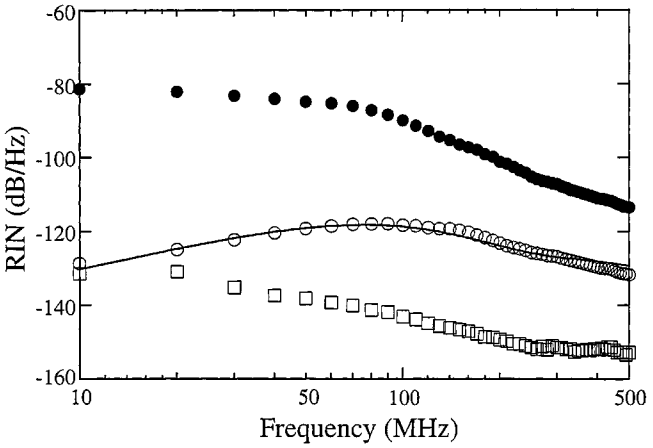

Fig. 4. Experimentally observed behavior of intrinsic relative intensity noise for the FP-LD (squares) and its center longitudinal mode (solid circles) and mode partition noise at the output of a 10-km long SM fiber (open circles). The light from the FP-LD is a continuous wave. The solid line shows the theoretical behavior of the mode partition noise under conditions identical to those used in the experiment.

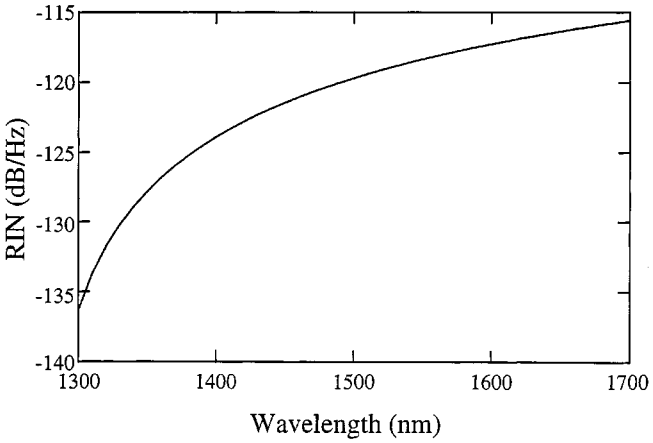

Fig. 5. Variation of mode partition noise with the center wavelength for a frequency of 90 MHz. The propagation fiber length is assumed to be 10 km.

noise. The solid line in this figure is the theoretical prediction of the mode partition noise obtained from (A6) given in the Appendix. In this calculation, the optical spectrum emitted from the FP-LD is assumed to obey a Gaussian distribution. It is very useful to estimate the mode partition noise because the calculated and experimental results agreed very well as shown in Fig. 4. As shown by (A6), the noise depends on the different time delays among longitudinal modes. Therefore, it is very important to understand the effect of the light source parameters, such as the center wavelength and the full width at half maximum (FWHM) of an optical spectrum.

1) Noise Dependence on Center Wavelength: Fig. 5 shows the theoretical mode partition noise as a function of center wavelength for a frequency of 90 MHz. There are three important assumptions in this calculation. First, the FWHM of an optical spectrum with a Gaussian distribution is 4.7 nm, and the mode spacing is 0.4 nm in all center wavelengths, as shown in Fig. 3. Second, all center longitudinal modes have the same RIN characteristics as those shown in Fig. 4. Third, the chromatic dispersion consists largely of material dispersion, and waveguide

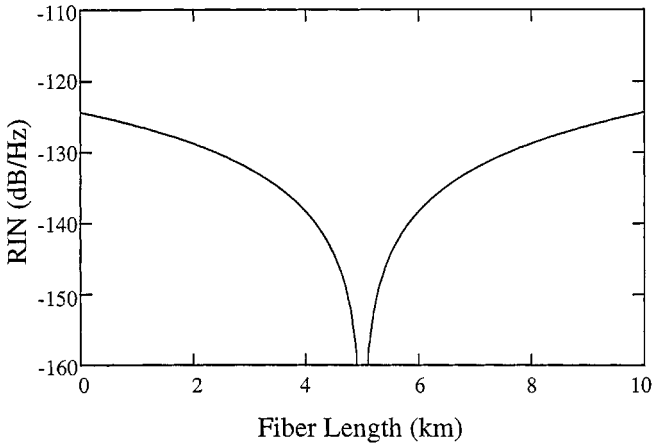

Fig. 6. Calculated mode partition noise as a function of fiber length for a frequency of 90 MHz. The conditions of this estimation are identical to those for the calculations shown in Fig. 5 excluding the transmission fiber length. A DCF compensates for the dispersion of a 5-km SM fiber.

dispersion contributes little. The dispersion D is obtained by using

$$D = -\frac{\lambda}{c}\frac{d^2 n}{d\lambda^2} \tag{7}$$

where λ is the wavelength in a vacuum, c is the speed of light in a vacuum, and n is the refractive index of the fiber core. The refractive index is assumed to obey the Sellmeier model as follows:

$$n(\lambda) = C_1 + C_2\lambda^2 + C_3\lambda^{-2} \tag{8}$$

with $C_1 = 1.450\,84$, $C_2 = -3.34 \cdot 10^9$, and $C_3 = 2.92 \cdot 10^{-15}$. When the center wavelength decreases from 1.65 to 1.55 μm, the noise is reduced by 2 dB, as shown in Fig. 5. The selection of the measurement wavelength from the 1.55-μm signal wavelength band is effective not only in terms of simplifying in-service measurement, but also in reducing noise. However, there is still a mode partition noise of -118 dB/Hz, since its wavelength does not coincide with the zero-dispersion wavelength of the measured SM fibers. There are two ways to reduce this noise. One is to use a dispersion compensator, such as a dispersion compensating fiber (DCF) or a chirped fiber Bragg grating (FBG) [7]. The other is to narrow the FWHM of the OTDR light source spectrum. The DCF cannot be applied to access networks with fiber length variations, because one DCF with a given compensation value cannot compensate for the dispersion values of all fibers, as shown in Fig. 6. In contrast, one FBG can compensate for any dispersion value. However, it is very difficult to design an FBG since the FP-LD spectrum is wide. Therefore, it is very effective to use an OTDR light source with a narrow spectrum.

2) Noise Dependence of Light Source Spectrum on FWHM: Fig. 7 shows the theoretical variation in the mode partition noise with the FWHM of the 1546-nm FP-LD spectrum. The remaining noise described in the above sub-section decreases when the FWHM becomes narrow. Since the linewidth of a distributed feedback laser diode (DFB-LD) is commonly less than 20 GHz, even though the laser is modulated directly, it is predicted that the use of the DFB-LD can suppress this

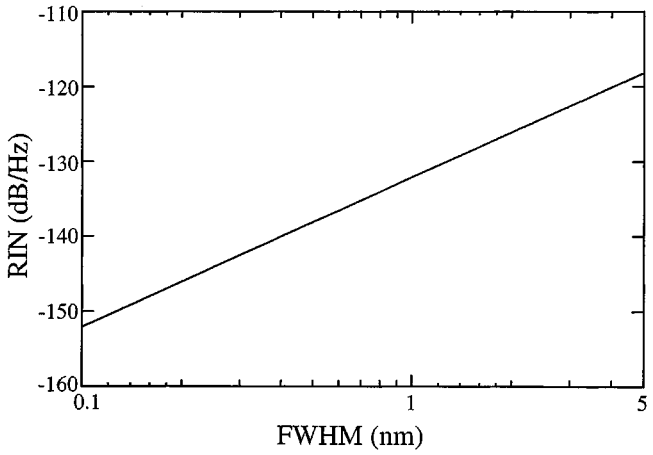

Fig. 7. Mode partition noise for FWHM of a light source at a frequency of 90 MHz. It is estimated under conditions identical to those of Fig. 5 except that the center wavelength is always 1546 nm and the mode spacing varies linearly with FWHM.

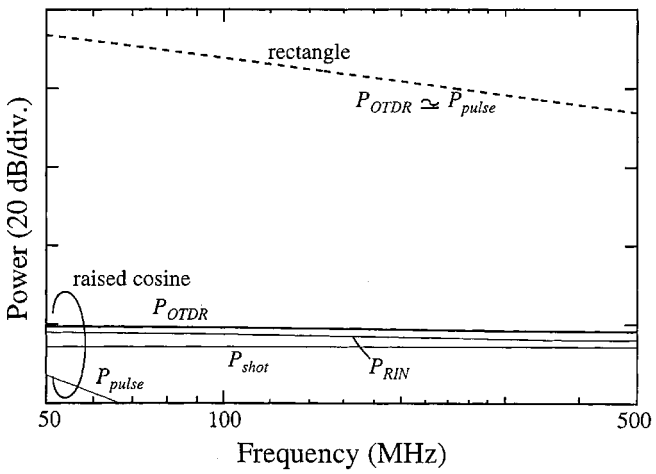

Fig. 8. Dependence of the additional noise power in $B_W = 4.2$ MHz on frequency for a 10-km long SM fiber. The raised cosine pulse from the DFB-LD has a 1-μs pulse width and a 430-μs pulse repetition cycle. The solid line shows the total additional noise power, and the light solid lines show its components. Moreover, the dashed line shows the pulse-induced noise power for a rectangular 1-μs pulse waveform. These values correspond to the total noise power caused by a conventional OTDR.

noise. In fact, when 1-μs pulses from a DFB-LD with a center wavelength of 1535 nm and a side mode suppressed ratio of -47 dBc propagated through a 10-km long SM fiber, there was no increase in the intensity noise resulting from the mode partition noise in the 50- to 500-MHz range. Therefore, a DFB-LD is useful as an OTDR light source, if its output power is high enough to measure a test fiber.

C. OTDR-Induced Total Noise Power

Fig. 8 shows the frequency characteristics of OTDR-induced noise obtained from (1) when an OTDR light with a pulse width of 1 μs and a pulse repetition cycle of 430 μs propagates through a 10-km SM fiber. The solid line shows the total noise power, when the OTDR pulse waveform is a raised cosine and its light source is the DFB-LD, described in the previous section. In this calculation, we estimated P_{RIN} from (6) using the RIN measurement results for the DFB-LD. In a conventional OTDR with a rectangular pulse and a 1.65-μm FP-LD, the pulse-induced noise power dominates the total noise power [5]. However, the use of the noise suppression technique means that the dominant factor becomes the RIN of the light source and the shot noise. The most noteworthy feature is that the total noise power is 70 dB less at a frequency of 90 MHz than that of a conventional OTDR. Since an in-service measurement system with a conventional OTDR needs an SWPF with a rejection ratio of -28 dB [5], it is possible to remove the SWPF from the system by using the novel OTDR with the proposed technique.

III. Experiment

We carried out in-service measurements to confirm the effectiveness of the proposed technique, and we describe our experimental results in this section. Moreover, we prove the effectiveness with calculated results.

A. Experimental Setup

Fig. 9 shows our experimental setup. We performed in-service measurements under the following conditions.

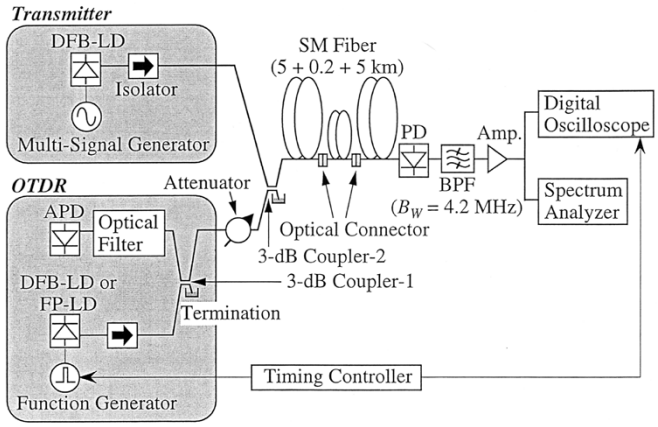

Fig. 9. Schematic illustration of the experimental setup we used to measure the CNR of a 40-channel AM-SCM video signal. The CNR is measured while an optical atteuator varies the received OTDR light power.

A 1558-nm DFB-LD was driven simultaneously by 40 AM subcarrier signals with frequencies of 91.25-325.25 MHz. The optical modulation index of each channel was 0.045. The optical video signal propagated via three SM fibers, with a total length of 10.2 km and an average chromatic dispersion of 18 ps/nm/km at the signal wavelength. The average signal light power received at a PD was -8 dBm. We measured the output RF signal through an electric bandpass filter (BPF) with $B_W = 4.2$ MHz from the PD with a spectrum analyzer and an oscilloscope. In contrast, OTDR light, with a pulse width of 1 μs and a repetition cycle of 430 μs, was emitted from an FP-LD with a center wavelength of 1629 nm or a 1535-nm DFB-LD. Raised cosine and rectangular pulses, as shown in Fig. 10, were generated by directly modulating the DFB-LD and the FP-LD, respectively. They were launched into the test fiber via an optical attenuator and a 3-dB coupler. The forward-propagated pulses entered the PD, and the back-reflected pulses were received at an avalanche photo diode (APD) in the OTDR. We installed an optical filter in

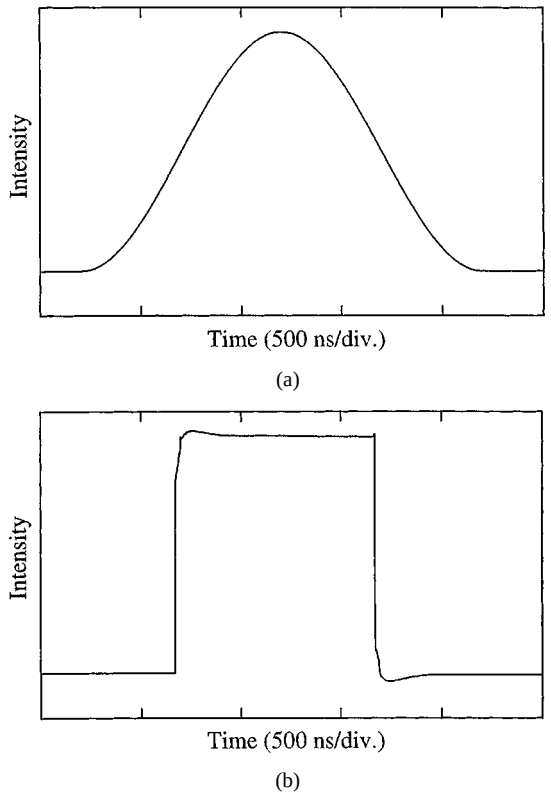

Fig. 10. Observed OTDR pulse waveforms of (a) raised cosine and (b) rectangle. These 1-μs pulses are obtained by modulating the light sources directly.

front of the APD to prevent the 1558-nm signals from entering it. Moreover, we installed optical isolators with an isolation of 50 dB in the output ports of all the lasers used in the experiments, because reflected light affects the intrinsic properties of lasers, such as intensity noise [8] and nonlinear distortion [9].

B. Experimental Results

1) CNR Measurement: We measured the CNR at a subcarrier frequency of 91.25 MHz, with different received OTDR light powers at the PD. We selected the measurement frequency on the grounds that the noise due to the OTDR light increases as the subcarrier frequency decreases, as shown in Fig. 8, and the lowest subcarrier frequency was 91.25 MHz in the experiments. When the OTDR light did not enter the PD, the CNR value was 44.2 dB. Fig. 11 shows the CNR measurement results for the two optical waveforms transmitted from the OTDR. In this figure, the circles and squares show the measured CNR values for the raised cosine and rectangular pulses, respectively. The CNR values of the raised cosine pulse were better than those of the rectangular one. The most noteworthy feature is that the video signal quality was unaffected, even though a raised cosine pulse with a peak power of 0 dBm entered the PD, as expected.

We also observed the CNR for other channels, excluding the 91.25-MHz channel, when the received peak power of the raised cosine pulse was 0 dBm. The result showed that all the signal characteristics were maintained, as we predicted from the noise power dependence on frequency shown in Fig. 8. Moreover, we considered whether or not the OTDR light affects the signal distortion, as investigated in [10]. This is because pump depletion occurs if the power transmitted through an optical fiber exceeds the Brillouin threshold, which is relatively low. However, neither the composite second-order (CSO) nor the composite triple-beat (CTB) increased, even though a raised cosine pulse with a peak power of 0 dBm propagated in the fiber, and both of these values were always less than -65 dBc. This is because the Brillouin threshold depends on the linewidth of the light source and fiber length. In general, the linewidth of the directly modulated light source is more than 100 MHz, which is wider than the Brillouin-gain bandwidth. Moreover, the used fiber length of 10 km is relatively short for the nonlinear effect, while it is long enough to distribute to customers' premises in access areas. As a result, the threshold exceeds 10 dBm, and the OTDR light does not contribute to an increase in the signal distortion. In fact, we observed no white-line on a TV-monitor, as shown in [5] when the 0-dBm raised cosine pulse entered the PD.

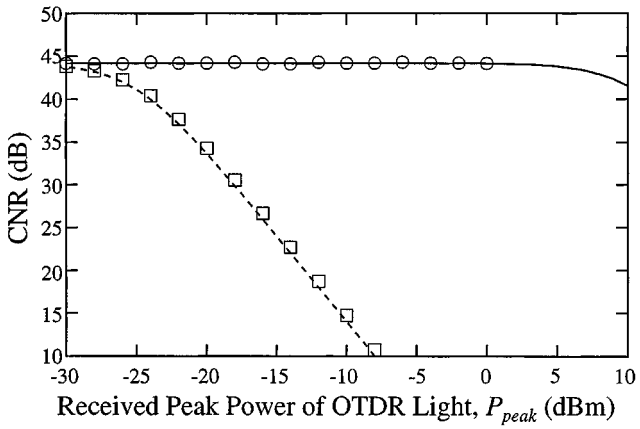

Fig. 11. Variation in CNR as a function of the received OTDR light power. Circles and squares show the measured CNR values for the raised cosine and rectangular pulses, respectively. The solid and dashed curves show the theoretically predicted CNR for the raised cosine and rectangular pulses, respectively. In this calculation for the rectangle, it is assumed that the total noise power is given by only pulse-induced noise.

In the presence of OTDR light at an ONU, CNR is given by

$$\mathrm{CNR}^{-1} = \mathrm{CNR}_0^{-1} + P_{\mathrm{OTDR}}/P_S \tag{9}$$

where CNR_0 is the value when the OTDR light is excluded, and P_S is the average received subcarrier signal power. P_S is written as

$$P_S = \frac{1}{2}(m \cdot \rho P_{ls})^2 R_D G, \tag{10}$$

where m is the optical modulation index per channel and P_{ls} is the average received signal light power at the ONU.

Fig. 11 shows the CNR estimated from (9) under the conditions listed in Tables I and II. The solid and dashed curves show the calculated CNR for the raised cosine and rectangular pulses, respectively. These results agreed with the experimental ones. It is interesting to note that the allowable received peak power increases to 7 dBm from -28 dBm when we use the noise suppression technique, while permitting the CNR to decrease by 1 dB. Therefore, the use of the technique can allow us to eliminate SWPFs from in-service measurements systems.

2) OTDR Performance: Fig. 12(a) and (b) show OTDR traces for raised cosine and rectangular pulses, respectively,

TABLE I
EXPERIMENTAL CONDITIONS FOR LIGHTWAVE SCM SYSTEM.

Subcarrier Frequencies	91.25 ~ 325.25 MHz
Number of Channels	40
Light Source	DFB-LD
Center Wavelength	1558 nm
Optical Modulation Index per Channel (m)	0.045
Transmission Line	10.2-km SM Fiber
Average Optical Received Power at ONU (P_{ls})	-8 dBm
CNR in absence of OTDR light (CNR_0)*	44.2 dB
Signal Bandwidth (B_W)	4.2 MHz

* at 91.25 MHz

TABLE II
EXPERIMENTAL CONDITIONS FOR OTDR.

Pulse Waveform	Raised Cosine	Rectangle
Light Source	DFB-LD	FP-LD
Center Wavelength	1535 nm	1629 nm
RIN of Light Source (RIN_1)*	-151 dB/Hz	-134 dB/Hz
RIN of Mode Partition Noise (RIN_2)*	—	-112 dB/Hz
Pulse Peak Power at Output Port of Isolator (P^0_{peak})	10 dBm	
Pulse Width (T_P)	1 μs	
Pulse Repetition Cycle (T_R)	430 μs	
Insertion Loss of Optical Filter	2 dB	
Minimum Detectable Power of APD (Pd)	-60 dBm	

* at 91.25 MHz

while the test fiber was in service. The dynamic ranges (DR) of both the OTDRs are about 18 dB, when considering the 3-dB insertion loss of coupler-2 shown in Fig. 9.

The DR can be estimated from [11]

$$\mathrm{DR} = \frac{P^0_{\mathrm{peak}} - R - C - P_d + \mathrm{SNIR}/2}{2} \quad [\mathrm{dB}] \qquad (11)$$

where

- P^0_{peak} peak power of the OTDR pulse at the output port of the isolator;
- R Rayleigh backscattering factor;
- C round-trip loss of 3-dB coupler-1 and the insertion loss of the optical filter;
- P_d minimum detectable power of the APD;
- SNIR improvement in the signal-to-noise ratio achieved by signal averaging.

When the OTDR properties shown in Table II, $R = 53$ dB and $\mathrm{SNIR} = 54$ dB are applied to the theoretical prediction, a DR of 18 dB is obtained from (11). This result is in good agreement with the experimental one. The amplitude fluctuation caused by the fading noise is measured in the fiber area of the OTDR trace with the raised cosine pulse, as shown in Fig. 12(a). By contrast, there is no fluctuation in the rectangular pulse, as shown in Fig. 12(b), because the OTDR light source is the FP-LD and

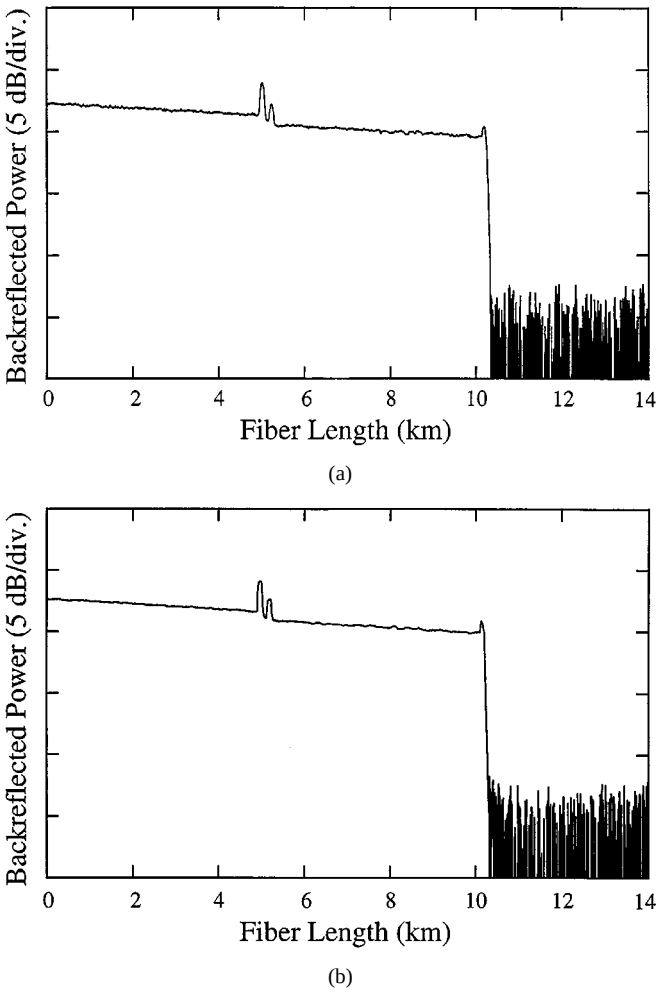

Fig. 12. OTDR traces of (a) raised cosine pulses and (b) rectangular pulses while the test fiber was in service. The traces were obtained by integrating the back-reflected light power 2^{18} times. The optical attenuator in front of OTDR was removed during the measurements.

it has multilongitudinal modes for a light spectrum. However, the fading noise can be reduced by using the frequency hopping technique with the DFB-LD as the OTDR light source [12]. Even though the pulse waveform is a raised cosine, the spatial resolution is estimated to be about 100 m from the full width at 1.5-dB maximum of the Fresnel reflection in Fig. 12(a). Moreover, Fig. 12(a) and (b) shows that the Fresnel reflection from optical connectors with a 0.2-km spacing can be resolved in both OTDRs. Therefore, we can confirm that the proposed OTDR provides the same performance as a conventional OTDR, in terms of DR and spatial resolution.

IV. LIMITATION OF SPATIAL RESOLUTION

To reduce the pulse-induced noise, the sidelobes of an OTDR pulse frequency spectrum are suppressed by shaping the pulse waveform. However, this technique is not very effective when the pulse width is reduced to enhance the spatial resolution of the OTDR. This is because the spectrum widens as the pulse width decreases, and the sidelobes are superimposed on the subcarrier frequency band in AM-SCM systems. In this section, we consider the pulse width limitation when using our proposed technique.

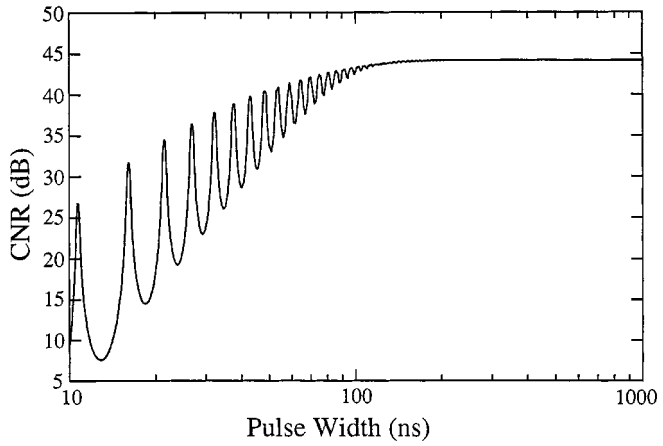

Fig. 13. Dependence of the CNR at a subcarrier frequency of 91.25 MHz on OTDR pulse width. All parameters are identical to those in Tables I and II except that the received peak power of the OTDR light is always 0 dBm.

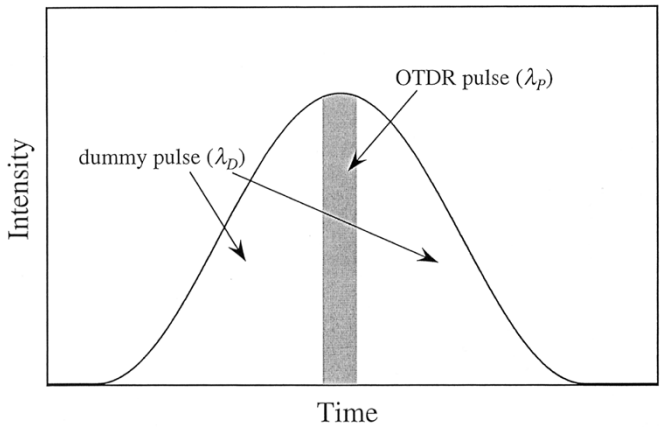

Fig. 14. Schematic illustration of quasiraised cosine pulse. λ_P and λ_D are the wavelengths of the OTDR pulse and the dummy pulse, respectively. These wavelengths are different from each other.

Fig. 13 shows the CNR variation for a raised cosine pulse as a function of pulse width. The CNR values are given by (9), and all parameters are identical to those in Tables I and II, except that the received OTDR peak power is always 0 dBm. The most notable feature is that the pulse width can be reduced to 100 ns, which corresponds to a spatial resolution of 10 m. We consider the following technique as a way of further enhancing the spatial resolution.

The OTDR sends out a quasiraised cosine pulse, with a wider pulse width. This pulse is composed of the narrower OTDR pulse and a complementary dummy pulse, as shown in Fig. 14. This causes the sidelobe of the composite wave to be greatly suppressed, while reducing the OTDR pulse width. Moreover, a wavelength is chosen for the dummy pulse, which is different from that of the OTDR pulse. This is so that only the backscattered light of the OTDR pulse can be detected by positioning an optical filter, which rejects the dummy pulse at the input port of the OTDR detector. By contrast, we must note that the dynamic range of the OTDR decreases with a decrease in OTDR pulse width, while the OTDR pulse peak power is kept constant. This is because the Rayleigh backscattering factor decreases, and the minimum detectable power of the OTDR receiver increases when the pulse width becomes narrow.

V. Conclusion

This paper proposed a novel in-service measurement technique, with an OTDR operating in a signal wavelength band for amplitude modulated vestigial sideband signal distribution systems employing the AM-SCM technique. By using the proposed technique, fiber line, splice and connector return losses for the signal can be estimated directly from the OTDR measurement results, because they can be measured in the same wavelength band as the signal. The new technique has two features designed to suppress the extra noise, which occurs when the OTDR light enters an optical network unit (ONU). One is to form the OTDR pulse into a raised cosine, in order to reduce the pulse-induced noise. The other is to use a distributed feedback laser diode (DFB-LD) as the OTDR light source, which contributes to a decrease in the mode partition noise.

We observed the CNR degradation in a 40-channel AM-SCM system operating at 1558 nm, caused by injecting an OTDR pulse into an ONU. In our experiments, the video quality was maintained by using a new OTDR with our proposed technique, even though an OTDR pulse with a peak power of 0 dBm entered the ONU. Moreover, there was no degradation in the spatial resolution or dynamic range of the OTDR.

In a conventional surveillance system, a short wavelength pass filter (SWPF) is installed in front of the ONU to prevent OTDR light from entering it. However, our technique makes it possible to eliminate the SWPF from the system, and is very effective in reducing the system cost.

Appendix
Analysis of Mode Partition Noise

The instantaneous optical power of the ith longitudinal mode a_i is given by the sum of its averaged optical power and its fluctuation, as shown in the following equation:

$$a_i(t) = \langle a_i \rangle + \int_{-\infty}^{\infty} A_i(f) \cdot e^{j2\pi ft}\, df \tag{A1}$$

where the angled brackets denote the time average and A_i represents the small fractions of the ith longitudinal mode around the stationary values in the frequency domain.

When the total power emitted from a light source is assumed to be

$$\sum_{i=1}^{N} a_i = 1 \tag{A2}$$

the mode partition noise RIN_2 at a distance of L in an optical fiber is given by

$$\begin{aligned}\mathrm{RIN}_2(f) &= \left\langle \left| \sum_{i=1}^{N} A_i(f) \cdot e^{-j2\pi f\tau_i} \right|^2 \right\rangle \\ &= \sum_{i=1}^{N} \langle A_i^2 \rangle + \sum_{i=1}^{N} \sum_{k>i}^{N} 2\cos(2\pi f(\tau_i - \tau_k)) \langle A_i A_k \rangle \end{aligned} \tag{A3}$$

with τ_i given by

$$\tau_i = (\lambda_i - \lambda_c)DL \tag{A4}$$

where

λ_i wavelength of the ith mode;
λ_c center wavelength of the light source;
D dispersion value of the fiber at λ_c.

From (A1) and (A2), the frequency components of the fluctuations have the following relation:

$$\sum_{i=1}^{N} A_i(f) = 0 \tag{A5}$$

and thus (A3) becomes

$$\begin{aligned} \mathrm{RIN}_2 &= \sum_{i=1}^{N} \left\langle A_i \left(1 - \sum_{k\neq i}^{N} A_k\right)\right\rangle \\ &\quad + \sum_{i=1}^{N}\sum_{k>i}^{N} 2\cos(2\pi f(\tau_i - \tau_k))\langle A_i A_k\rangle \\ &= K(f)\sum_{i=1}^{N}\sum_{k>i}^{N} \eta_{ik}(f)\langle a_i\rangle\langle a_k\rangle \end{aligned} \tag{A6}$$

where

$$\eta_{ik} = 2\{1 - \cos(2\pi f(\tau_i - \tau_k))\} \tag{A7}$$

and

$$K = -\frac{\sum_{i=1}^{N}\sum_{k>i}^{N}\eta_{ik}\langle A_i A_k\rangle}{\sum_{i=1}^{N}\sum_{k>i}^{N}\eta_{ik}\langle a_i\rangle\langle a_k\rangle}. \tag{A8}$$

Since we assume that every longitudinal mode consists of a stimulated emission, not a spontaneous emission, the relation of

$$\langle A_i A_k\rangle = \alpha\langle a_i\rangle\langle a_k\rangle \quad (\alpha = \text{constant}, i \neq k) \tag{A9}$$

will hold for any stimulated emission [13]. Therefore, K can be written as

$$K = -\frac{\sum_{i=1}^{N}\sum_{k>i}^{N}\langle A_i A_k\rangle}{\sum_{i=1}^{N}\sum_{k>i}^{N}\langle a_i\rangle\langle a_k\rangle} = -\frac{\langle A_i A_k\rangle}{\langle a_i\rangle\langle a_k\rangle}. \tag{A10}$$

Since (A2) and (A5) give the relations of

$$\sum_{i=1}^{N}\langle a_i\rangle = 1 \tag{A11}$$

and

$$\left\langle \left(\sum_{i=1}^{N} A_i\right)^2 \right\rangle = 0 \tag{A12}$$

respectively, (A10) yields

$$K(f) = \frac{\langle A_i^2\rangle}{\langle a_i\rangle - \langle a_i\rangle^2} = \mathrm{RIN}_c(f)\cdot\frac{1}{\langle a_c\rangle^{-1} - 1} \tag{A13}$$

where RIN_c and a_c are the relative intensity noise and optical power of the center mode, respectively.

REFERENCES

[1] W. I. Way, "Subcarrier multiplexed lightwave system design considerations for subscriber loop applications," *J. Lightwave Technol.*, vol. 7, pp. 1806–1818, Nov. 1989.

[2] S. L. Woodward, X. Lu, T. E. Darcie, and G. E. Bodeep, "Technique for the reduction of optical beat interference in subcarrier multiplexed systems," *OFC'96 Tech. Dig.*, pp. 213–214, 1996.

[3] K. Maeda and S. Morikawa, "Study of BER of 64-QAM signal and OMI-window of feasible operation in analog/digital hybrid SCM transmission systems," *J. Lightwave Technol.*, vol. 17, pp. 1011–1017, June 1999.

[4] S. Furukawa, H. Suda, F. Yamamoto, Y. Koyamada, T. Kokubun, and I. Takahashi, "Optical fiber line test and management system for passive double star networks and WDM transmission systems," in *44th. IWCS Proc.*, 1995, pp. 640–648.

[5] F. Yamamoto and T. Horiguchi, "Allowable received OTDR light power for in-service measurement in lightwave SCM systems," *J. Lightwave Technol.*, vol. 18, pp. 286–294, Mar. 2000.

[6] K. Peterman and G. Arnold, "Noise and distortion characteristics of semiconductor lasers in optical fiber communication systems," *IEEE J. Quantum Electron.*, vol. 18, pp. 543–555, Apr. 1982.

[7] K. O. Hill, S. Theriault, B. Malo, F. Bilodeau, T. Kitagawa, D. C. Johnson, J. Albert, K. Takiguchi, T. Kataoka, and K. Hagimoto, "Chirped in-fiber Bragg grating dispersion compensators: Linearization of the dispersion characteristics and demonstration of dispersion compensation in a 100 km, 10 Gbit/s optical fiber link," *Electron. Lett.*, vol. 30, no. 21, pp. 1755–1756, 1994.

[8] O. Hirota, Y. Suematsu, and K. S. Kwok, "Properties of intensity noises of laser diodes due to reflected waves from single-mode optical fibers and its reduction," *IEEE J. Quantum Electron.*, vol. 17, pp. 1014–1020, June 1981.

[9] K. Kikushima and Y. Suematsu, "Nonlinear distortion properties of laser diode influenced by coherent reflected waves," *Trans. IEICE Japan*, vol. 67, pp. 19–25, Jan. 1984.

[10] Y. K. Chen, Y. R. Wu, C. H. Chang, C. C. Lee, F. Y. Tsai, C. S. Wang, and Y. K. Tu, "Baseband video distortion due to on-line OTDR monitoring at 1.65 μm with negligible CNR/CSO/CTB degradation," in *OFC'98 Tech. Digest*, 1998, pp. 87–89.

[11] T. Sato, T. Horiguchi, Y. Koyamada, and I. Sankawa, "A 1.6 μm band OTDR using a synchronous raman fiber amplifier," *IEEE Photon. Technol. Lett.*, vol. 4, pp. 923–924, Aug. 1992.

[12] H. Izumita, Y. Koyamada, S. Furukawa, and I. Sankawa, "Stochastic amplitude fluctuation in coherent OTDR and a new technique for its reduction by stimulating synchronous optical frequency hopping," *J. Lightwave Technol.*, vol. 15, pp. 267–278, Feb. 1997.

[13] K. Ogawa and R. S. Vodhanel, "Measurements of mode partition noise of laser diodes," *IEEE J. Quantum Electron.*, vol. 18, pp. 1090–1093, July 1982.

Fumihiko Yamamoto was born in Yamaguchi, Japan, on January 25, 1966. He received the B.E. and M.E. degrees in mechanical engineering from Kyusyu University, Fukuoka, Japan, in 1989 and 1991, respectively.

In 1991, he joined NTT Transmission Systems Laboratories, Ibaraki, Japan, where he has been engaged in research and development on in-service measurement technologies in optical access networks. He is now a Research Engineer of NTT Access Network Service Systems Laboratories, Ibaraki, Japan, and works on WDM optical network design in metropolitan and local areas.

Tsuneo Horiguchi (M'87-SM'96) was born in Tokyo, Japan, on June 5, 1953. He received B.E. and Dr. Eng. degrees from The University of Tokyo, Tokyo, Japan, in 1976 and 1988, respectively.

In 1976, he joined the Ibaraki Electrical Communication Laboratories, NTT, where he worked on the measurement of the transmission characteristics of optical fiber cable. Since 1988, he has worked in the field of optical fiber distributed sensing. He is presently the Executive Manager of the Advanced Transmission Media Project, NTT Access Network Service Systems Laboratories, Ibaraki, Japan.

Dr. Horiguchi is a member of the Institute of Electronics, Information and Communication Engineers (IEICE) of Japan, the Optical Society of Japan, and the Optical Society of America (OSA).